Article

Immunity

Affinity-independent memory B cell origin of the early antibody-secreting cell response in naive individuals upon SARS-CoV-2 vaccination

Graphical abstract

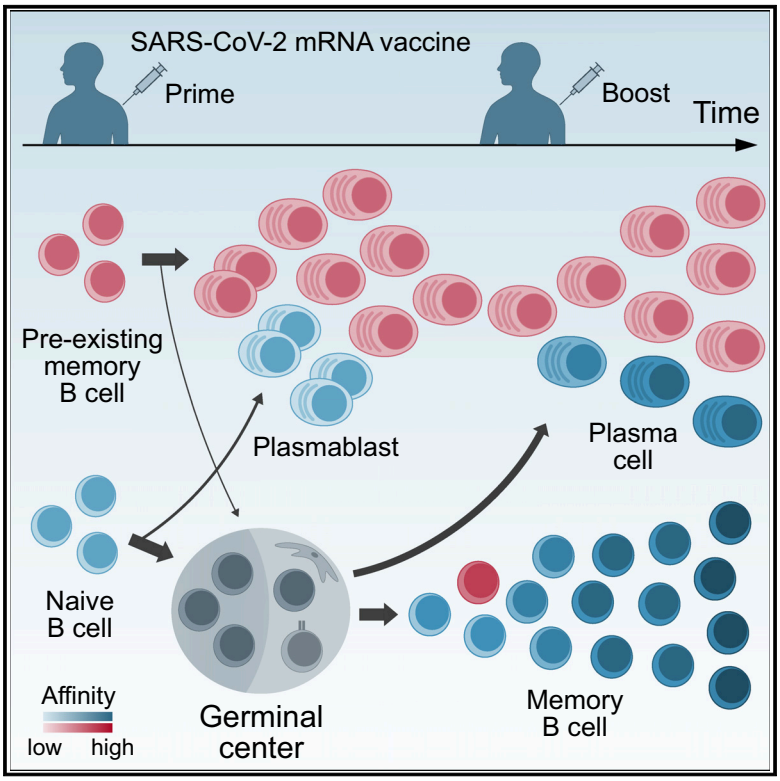

Authors

Zhe Li, Anna Obraztsova, Fuwei Shang, ..., Erec Stebbins, Rajagopal Murugan, Hedda Wardemann

Correspondence

a.obraztsova@dkfz.de (A.O.), h.wardemann@dkfz.de (H.W.)

In brief

Memory B cells dominate recall responses, but how they react to novel antigens is not well understood. Li and Obraztsova et al. show that MBCs with similar antigen reactivity as those of naive B cells rapidly differentiate into ASCs without signs of germinal center re-entry, whereas affinity maturation of naive B cells underlies improvements in humoral immunity to novel antigens.

Highlights

- SARS-CoV-2 mRNA vaccination activates naive and pre-existing MBCs in naive individuals
- S-reactive naive, but not pre-existing, MBCs show signs of strong affinity maturation
- Despite low S reactivity, pre-existing MBCs dominate the early ASC response
- High-affinity anti-S MBCs and ASCs develop from naive, not MBC, precursors

Li et al., 2024, Immunity *57*, 2191–2201
September 10, 2024
https://doi.org/10.1016/j.immuni.2024.07.023

CellPress

Immunity

CellPress
OPEN ACCESS

Article

Affinity-independent memory B cell origin of the early antibody-secreting cell response in naive individuals upon SARS-CoV-2 vaccination

Zhe Li,[1,8] Anna Obraztsova,[1,2,8,*] Fuwei Shang,[3,4] Opeyemi Ernest Oludada,[1,2,6] Joshua Malapit,[1,2] Katrin Busch,[3] Monique van Straaten,[5] Erec Stebbins,[5] Rajagopal Murugan,[1,7] and Hedda Wardemann[1,9,*]

[1]B Cell Immunology, German Cancer Research Center, Heidelberg 69120, Germany
[2]Faculty of Biosciences, University of Heidelberg, Heidelberg 69120, Germany
[3]Cellular Immunology, German Cancer Research Center, Heidelberg 69120, Germany
[4]Faculty of Medicine, University of Heidelberg, Heidelberg 69120, Germany
[5]Structural Biology of Infection and Immunity, German Cancer Research Center, Heidelberg 69120, Germany
[6]Present address: Department of Immunology, University of Toronto, Toronto, ON M5S 1A8, Canada
[7]Present address: Leiden University Center for Infectious Diseases, Leiden University Medical Center, Leiden, 2333 ZA, the Netherlands
[8]These authors contributed equally
[9]Lead contact
*Correspondence: a.obraztsova@dkfz.de (A.O.), h.wardemann@dkfz.de (H.W.)
https://doi.org/10.1016/j.immuni.2024.07.023

SUMMARY

Memory B cells (MBCs) formed over the individual's lifetime constitute nearly half of the circulating B cell repertoire in humans. These pre-existing MBCs dominate recall responses to their cognate antigens, but how they respond to recognition of novel antigens is not well understood. Here, we tracked the origin and followed the differentiation paths of MBCs in the early anti-spike (S) response to mRNA vaccination in SARS-CoV-2-naive individuals on single-cell and monoclonal antibody levels. Pre-existing, highly mutated MBCs showed no signs of germinal center re-entry and rapidly developed into mature antibody-secreting cells (ASCs). By contrast, and despite similar levels of S reactivity, naive B cells showed strong signs of antibody affinity maturation before differentiating into MBCs and ASCs. Thus, pre-existing human MBCs differentiate into ASCs in response to novel antigens, but the quality of the humoral and cellular anti-S response improved through the clonal selection and affinity maturation of naive precursors.

INTRODUCTION

A hallmark of the adaptive immune system is the formation of immunological memory. Long-lived humoral immunity is mediated by two types of cells, long-lived antibody-secreting plasma cells (PCs) that maintain stable antigen-specific serum immunoglobulin (Ig) levels over time and memory B cells (MBCs) that can rapidly differentiate into antibody-secreting cells (ASCs) upon re-exposure to the same antigen.[1–3] Although any recall response will also activate antigen-reactive naive B cells that encounter the antigen for the first time, their affinity is usually lower than that of MBCs that have undergone extensive affinity maturation in germinal center (GC) reactions during the primary response.[1,4] Consequently, MBCs dominate humoral recall responses initiated by the same pathogen. The fast production of MBC-derived, high-affinity serum antibodies mediates immediate and effective protection from infections with pathogens that show little antigenic variation.[5]

In humans, class-switched and non-class-switched MBCs constitute nearly half of the circulating B cell pool.[6] All subsets express mutated Ig genes with clear signs of antigen-mediated selection, suggesting that the cells show high affinity for foreign antigens that the host encountered earlier in life.

Because MBCs develop throughout ongoing immune responses, their antigen-receptor repertoire shows a broad range of affinities likely enabling flexibility in recall responses to antigenically distant stimuli.[7] Indeed, MBCs with reactivity to seasonal human coronaviruses (HCoVs) participate in infection- or vaccination-induced anti-severe acute respiratory syndrome coronavirus 2 (SARS-CoV-2) responses if their antigen receptors show strong cross reactivity with the viral spike (S) proteins, predominantly the conserved S2 subunit.[8,9] Direct lymph node sampling showed that cross-reactive MBCs can participate in GC reactions along with naive B cells.[10–12] However, to what extent pre-existing MBCs participate in the anti-SARS-CoV-2 response compared with naive B cells and the degree to which they affinity mature over time in individuals with no prior exposure to the virus is not well understood. Studies in mice have shown that the frequency of MBCs in secondary GCs is low compared with naive B cells,[13–17] suggesting that MBCs re-enter GCs rarely, but whether the same is true in humans is not known. A better understanding of the question of whether MBCs undergo efficient

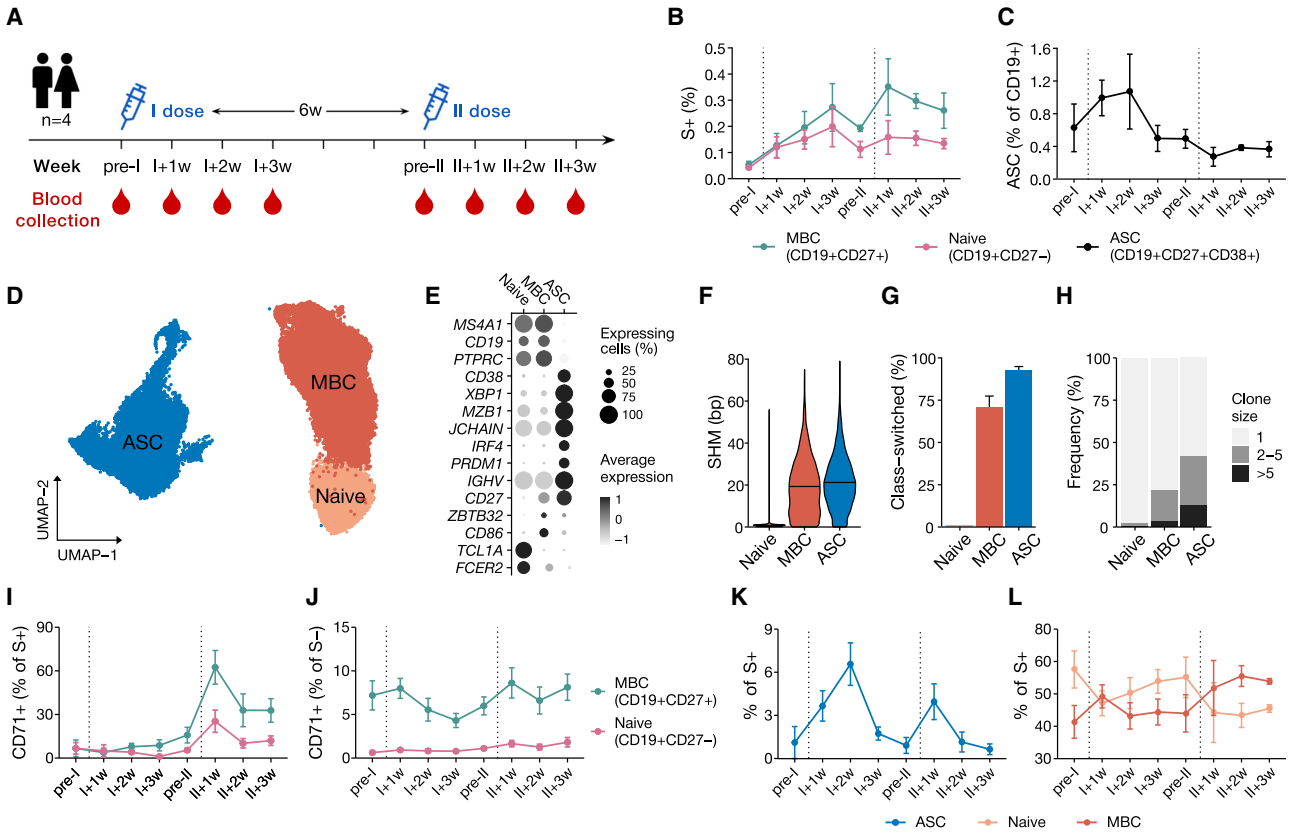

Figure 1. Naive and pre-existing MBCs respond to SARS-CoV-2 mRNA vaccination in naive individuals

(A) Study design. I, first dose; II, second dose; pre-I and pre-II, the day before the first and the second vaccination; 1, 2, and 3 weeks after vaccination.

(B) The frequency of S+ B cells in memory (CD19+CD27+) and naive (CD19+CD27−) populations from PBMCs over time was measured by flow cytometry.

(C) Frequency of ASCs as a percent of total CD19+ cells over time.

(D–H) Identification of antibody-secreting cells (ASCs), memory B cells (MBCs), and naive B cells sorted from peripheral blood samples from all time points based on single-cell transcriptome and Ig gene usage analysis. (D) UMAP projection of single-cell transcriptional profiles colored by population defined through transcriptome analysis. (E) Expression profile of selected marker genes. (F) *IGHV* + *IGK/LV* somatic hypermutation (SHM) counts across the indicated cell populations. (G) Class-switched antibody frequency. (H) Clone size distribution.

(I and J) Frequency of CD71+ cells in S+ (I) and S− (J) naive (CD19+CD27−) and memory B cells (CD19+CD27+) as measured by flow cytometry.

(K and L) Frequency of antibody-secreting (K) and B cell (L) populations in S+ cells over time based on the transcriptome. Dots show average frequency across the volunteers and error bars show SEM. Dotted vertical lines indicate prime and boost.

See also Figure S1.

secondary affinity maturation is critical for the development of vaccines against pathogens with low frequency of potent naive precursors that strongly rely on the development of antibodies with high somatic hypermutation (SHM) loads.

To address this question, we studied the evolution of the anti-S protein response in SARS-CoV-2-naive individuals over two vaccinations with mRNA. Despite similar antigen-receptor-mediated S binding at the onset of the response compared with naive B cells, pre-existing S-reactive MBCs quickly differentiated into ASCs. By contrast, newly developing MBCs derived from activated S-reactive naive B cells showed evidence of efficient affinity maturation in GC reactions upon class-switching to IgG. The data demonstrate the intrinsic propensity of MBCs to drive immediate humoral immune responses independently of their antigen-binding strength through differentiation into ASCs. Although rare pre-existing MBCs may participate in GC reactions, the quality of the anti-S IgG memory antibody response to mRNA vaccination is based on the antigen-mediated activation and affinity maturation of naive B cells likely during GC reactions.

RESULTS

Naive and pre-existing MBCs respond to SARS-CoV-2 mRNA vaccination in naive individuals

To follow the development of the anti-S B cell response upon mRNA vaccination, we collected plasma and peripheral blood mononuclear cells (PBMCs) from four healthy SARS-CoV-2-naive volunteers (V1–4; Table S1) directly before (pre) and 1, 2, and 3 weeks after the first (I) and second (II) vaccination with Comirnaty (Figure 1A). All donors responded with strong humoral IgG, but not IgM or IgA responses, against the viral S protein, especially after the boost (Figures S1A–S1C). The lack of IgA titers and delayed IgG response compared with an individual with prior coronavirus disease (V5) confirmed that these donors were SARS-CoV-2 naive. Indicative of the ongoing immune response,

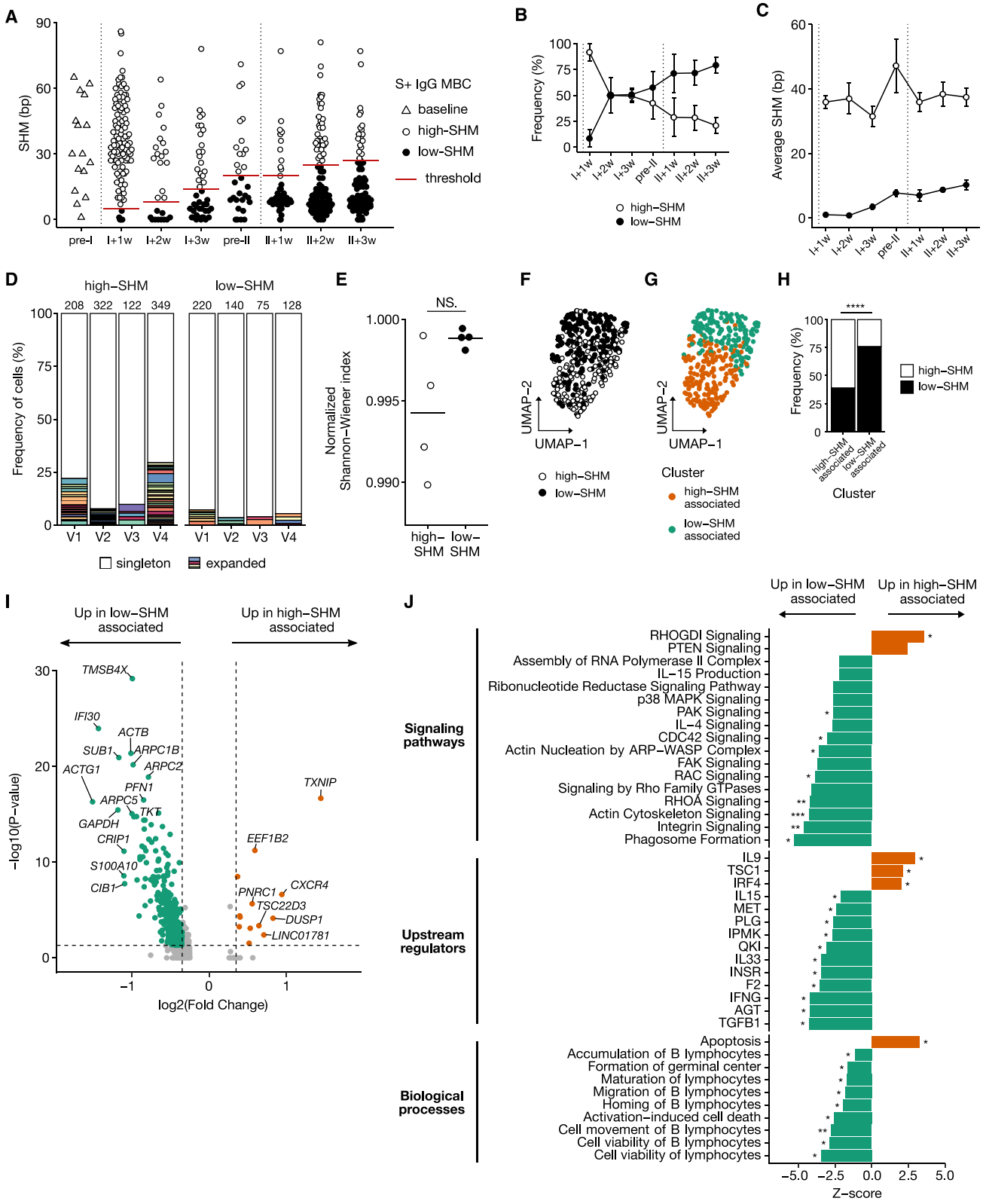

Figure 2. Low-SHM, but not high-SHM, S+ IgG MBCs display signs of ongoing GC reaction

(A) *IGHV* + *IGK/LV* SHM counts in S+ IgG MBCs. Dotted vertical lines indicate prime and boost.

(B) Frequency of low- and high-SHM MBCs over time.

(legend continued on next page)

flow cytometric analyses showed an increase in S+ naive B cells (CD19+CD27−S+) and MBCs (CD19+CD27+S+) after the prime and boost vaccinations and of ASCs (CD19+CD27+CD38+) predominantly after the prime (Figures 1B and 1C). Prior to the vaccination, S+ MBCs were detected in all donors, in line with previous reports[18,19] (Figures 1B and S1D).

To characterize the response more deeply, we sorted these populations using barcoded S baits and performed transcriptome and Ig gene analyses (Figures 1D–1H). We included the activation marker CD71[20] and also isolated S−CD71+ naive B cells and MBCs to capture recently activated cells whose bait binding was below the flow cytometric detection threshold (Figure S1E). Transcriptome and Ig gene analysis of the pooled cells confirmed the cellular identity of the sorted populations independently of the sampling time point (Figures 1E–1H and S1F). ASCs were identified by high expression of *CD38, IRF4*, and *IGHV* and highly mutated and class-switched Ig genes and showed clear signs of clonal expansion (Figures 1E–1H). MBCs were overall more similar to naive B cells in their expression profile but expressed *CD27*, the activation marker *CD86*, and showed signs of clonal expansion (Figures 1E and 1H). As expected, their Ig genes were highly mutated and predominantly class-switched (Figures 1F and 1G). A fraction of S+ MBC clones that were detected before the vaccination were also present at later time points, likely reflecting the ongoing participation of these pre-existing MBCs in the anti-SARS-CoV-2 response (Figure S1G). The frequency of S+CD71+ naive B cells and MBCs increased with time, especially after the boost, compared with little change in the S− populations (Figures 1I and 1J). Independently of their S− reactivity, CD71+ cells were more frequent among MBCs than naive B cells, indicative of a higher baseline activation status (Figure 1J). The transcriptome analysis confirmed the higher expression of *TRFC* encoding for CD71 in MBCs compared with naive B cells, although only the S+*TRFC*+ subset reflected the vaccination-induced changes detected by flow cytometry (Figure S1H). Because S−CD71+ naive B cells and MBCs showed no evidence of active participation in the vaccine response, and might therefore reflect bystander activation, we focused all further analyses on S+ cells.

S+ ASCs were overall rare, presumably due to their low surface B cell antigen receptor (BCR) expression. Nevertheless, their frequency increased after each vaccination (Figure 1K). Prior to and at all time points post vaccination, the S+ B cell pool comprised naive B cells and MBCs (Figure 1L). Before and after the first vaccine dose, naive B cells constituted the majority of S+ cells, whereas MBCs dominated the response after the boost, likely reflecting the ongoing differentiation of antigen-reactive naive precursors into MBCs (Figure 1L).

Collectively, the data show that mRNA vaccination recruited not only S-reactive naive B cells into the response but also pre-existing S-reactive MBCs and induced the development of S+ and S− ASCs along with strong humoral anti-S IgG responses after the boost.

Low-SHM, but not high-SHM, IgG MBCs show signs of recent GC reaction participation

To dissect the contribution of newly generated and pre-existing MBCs to the anti-S response in more detail, we tracked the mutation load of S+ IgG MBCs. At I + 1 week, the vast majority (95%) of S+ IgG MBCs were highly mutated, with SHM counts comparable with those of pre-vaccination MBCs (Figure 2A). Only few cells were unmutated or lowly mutated at this early time point, but their numbers increased by II + 1 week, suggesting that newly recruited naive B cells had class-switched to IgG and entered the MBC pool (Figure 2B). To assess the contribution of these two S+ IgG MBC subsets to the response over time, we separated S+ IgG MBCs with no or low SHM counts from those with high SHM counts (referred to as low-SHM MBCs and high-SHM MBCs, respectively) based on the near bimodal distribution of their SHM load (Figures 2A and S2A). Low-SHM IgG MBCs accumulated SHM and increased almost 10-fold with time, from 8.3% at I + 1 week to 79.2% at II + 3 weeks, likely reflecting their export from ongoing GC reactions (Figures 2B and 2C). Although not statistically significant due to the highly polyclonal nature of the response, the frequency of clonally related IgG and IgM cells was indeed higher among low-SHM (16.7%, 2/12) compared with high-SHM (6.8%, 4/59) MBCs, suggesting that naive B cells differentiated into MBCs and class-switched to IgG before hypermutating their Ig genes. By contrast, lowly mutated IgM MBCs were detected with similar frequency at all sampling points and showed no change in SHM load over time, indicating that these cells did not undergo Ig gene diversification in response to the vaccination (Figures S2B–S2D).

The average SHM count in high-SHM IgG MBCs remained stable, even within large persistent clones (Figures 2C and S2E), supporting the notion that these cells originated from different precursors than the low-SHM IgG subpopulation. Indeed, we observed little clonal overlap (n = 7) between expanded B cell clones in low-SHM (n = 36) and high-SHM (n = 108) MBCs, and we identified higher numbers of expanded B cell clones with longer tree branches reflecting a longer Ig gene diversification history and lower clonal diversity in high-SHM compared with low-SHM MBCs (Figures 2D, 2E, S2F, and S2G). The two populations also differed in their transcription profiles (Figures 2F–2H). Upregulated genes and signaling pathways linked to low-SHM MBCs were associated with cytoskeleton

(C) Average SHM count over time.
(D) Clonal expansion of low- and high-SHM MBCs.
(E) Clonal diversity. Each dot represents one donor.
(F and G) UMAP projection of high- and low-SHM S+ IgG MBCs colored by SHM load (F) or cluster defined by unsupervised transcriptome clustering (G).
(H) Frequency of high- and low-SHM cells in the transcriptome clusters.
(I) Genes differentially expressed between low- and high-SHM-associated clusters.
(J) Signaling pathways and transcriptional programs enriched in genes differentially expressed between low- and high-SHM-associated clusters. NS, not significant, *$p < 0.05$, **$p < 0.01$, ***$p < 0.001$, ****$p < 0.0001$, two-tailed Mann-Whitney test (E), Pearson's chi-squared test with Yates' continuity correction (H), Fisher's exact test (J). Error bars display SEM (B–C).
See also Figure S2.

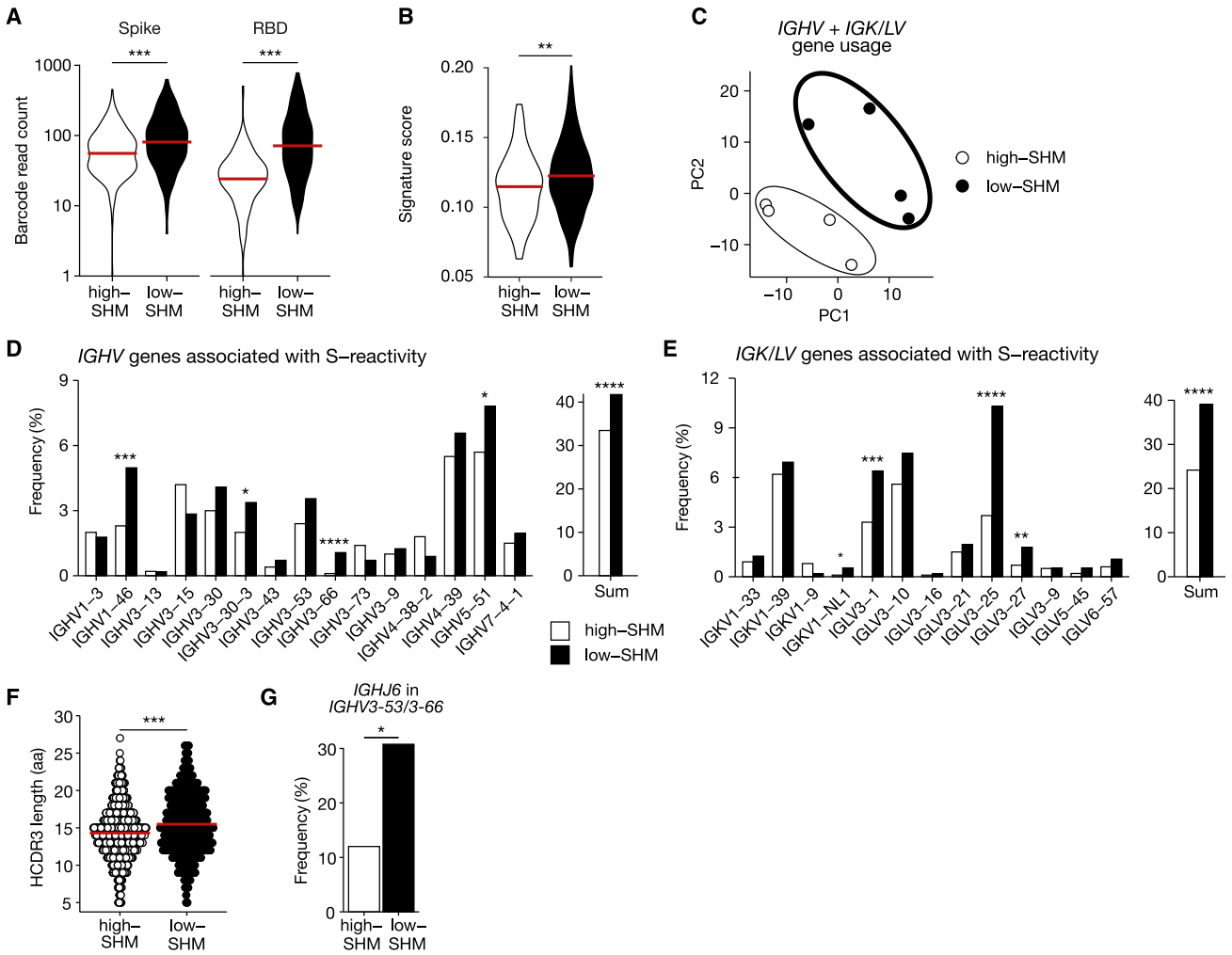

Figure 3. Features associated with S binding are enriched in antibodies of low-SHM S+ MBCs

(A) Read counts of spike and RBD tetramer barcodes in S+ IgG MBCs.

(B) BCR signaling pathway gene expression in S+ IgG MBCs.

(C–F) Ig-variable segment gene usage of S+ MBCs. (C) Principal component analysis (PCA) on paired-chain V gene usage (dots represent MBC populations from individual donors). (D) Frequency of individual *IGHV* genes associated with S binding (left) or their pooled frequency (right). (E) Frequency of individual *IGK/LV* genes associated with S binding (left) or their pooled frequency (right). (F) HCDR3 length distribution in S+ MBCs.

(G) Frequency of *IGHJ6* usage in cells using *IGHV3-53* or *IGHV3-66* in S+ MBCs. *$p < 0.05$, **$p < 0.01$, ***$p < 0.001$, ****$p < 0.0001$, two-tailed Mann-Whitney test (A, B, and F), exact binomial test with Benjamini-Hochberg correction for multiple testing (D, E, and G).

remodeling (*ACTB, ACTG1, PFN1, ARPC2*, and *ARPC1B*), cell motility, adhesion, and proliferation (RhoA, Cdc42, Rac, Pak, Fak, Actin, and Integrin signaling), as well as T cell help, B cell activation, GC formation and viability (IL-4, p38 MAPK, IL-15 and IFNγ signaling)[21,22] suggesting that these cells are recent GC emigrants (Figures 2I and 2J). By contrast, upregulated genes associated with high-SHM MBCs were mostly linked to PC differentiation and apoptosis (*TXNIP*, IRF4, and IL-9 signaling).[23,24]

We conclude that S+ low-SHM IgG MBCs develop from naive precursors that undergo Ig gene diversification and accumulate in the S+ IgG MBC pool with time. These cells are not related to pre-existing S+ IgG MBCs with high SHM counts, which likely developed prior to the vaccination, lack signs of ongoing affinity maturation, and express genes associated with PC differentiation.

Naive B cell-derived but not pre-existing MBCs show signs of anti-S-affinity maturation

Next, we determined whether high- and low-SHM IgG MBCs differed in their S binding based on barcode read counts and signaling pathway gene expression scores, respectively (Figures 3A and 3B). Low-SHM IgG MBCs showed on average higher S and receptor-binding domain (RBD) reactivity and stronger signs of BCR activation than high-SHM MBCs. Both populations also differed in their paired V gene usage (Figure 3C). Low-SHM MBCs showed a strong enrichment of *IGHV, IGKV*, and *IGLV* genes and Ig gene features associated with S reactivity (Figures 3D and 3E), including antibodies with long HCDR3[25,26] and *IGHV3-53* or *IGHV3-66* segments paired with *IGHJ6* that frequently encode high-affinity anti-RBD antibodies[27] (Figures 3F and 3G).

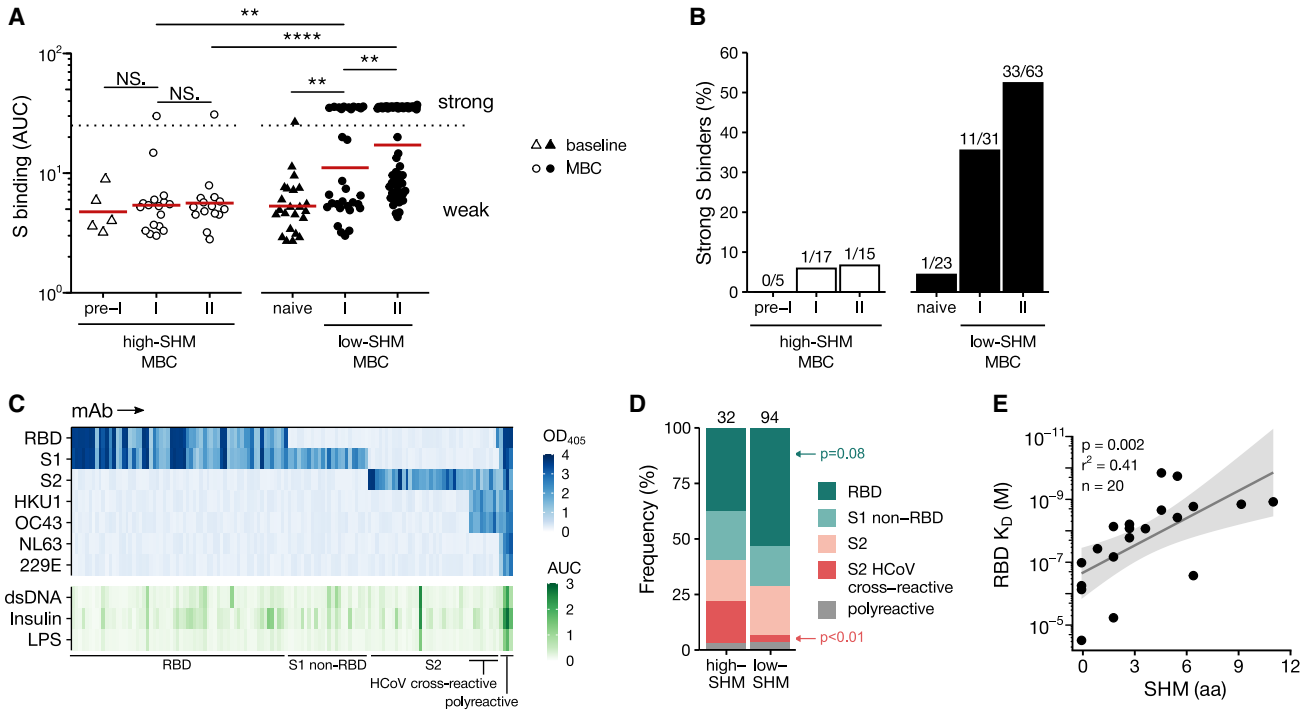

Figure 4. Antibodies of low-SHM IgG MBCs are better S binders that are improving over time

(A and B) ELISA area under the curve (AUC) values (A) and frequencies of strong S binding mAbs (B) in low- and high-SHM S+ IgG MBCs separated by isolation time point (I, after first vaccination; II, after second vaccination) and in naive B cells. Red lines show average, dotted horizontal line shows threshold for strong-binding mAbs. Numbers on top of the bars show the numbers of strong binders over the total number of S-binding mAbs.

(C) mAb reactivity profiles. Binding to SARS-CoV-2 RBD, S1, and S2, and to S protein from HKU1, OC43, NL63, and 229E was measured using high-sensitivity ELISA.

(D) Distribution of reactivity profiles among mAbs cloned from high- and low-SHM IgG MBCs. Arrows indicate comparisons of the frequency of RBD (green) and S2 HCoV cross-reactive mAbs among high- and low-SHM MBCs using exact binomial test.

(E) RBD binding affinity of strongly RBD-binding low-SHM IgG mAbs versus total *IGHV* + *IGKV/IGLV* SHM counts. Data are representative of at least two independent experiments. $^{**}p < 0.01$, $^{****}p < 0.0001$, two-tailed Mann-Whitney test (A), F-test (E).

See also Figure S3.

To evaluate the binding strength and epitope specificity of low- and high-SHM MBCs, we cloned and expressed 141 monoclonal antibodies (mAbs) from S+ IgG MBCs and 25 mAbs from S+ naive B cells isolated at different time points after the vaccination (Table S2). We expected mAbs from MBCs to have low binding affinity and used a sensitive ELISA based on the pre-incubation of the test mAbs with the polyclonal secondary antibody prior to addition of the formed complexes to the plate-bound antigen. Using this protocol, we identified a small fraction (7%) of non-S-binding mAbs that likely reflect the low experimental noise inherent in the bait-based cell isolation strategy that were excluded from all further analyses (Figure S3A). All other mAbs showed weak to high S binding in a standard ELISA (Figure 4A). Consistently in all donors, mAbs from low-SHM IgG MBCs showed on average higher antigen binding compared with mAbs from high-SHM IgG MBCs already after the prime (Figures 4A and S3B). Their binding strength and the frequency of strong binders increased after the boost, whereas that of high-SHM IgG MBCs remained similar to naive B cells (Figures 4A and 4B). mAbs cloned from high- and low-SHM MBCs recognized RBD and non-RBD epitopes in the S1 and S2 domains, including a few polyreactive mAbs that recognized structurally diverse non-SARS-CoV-2 antigens, such as DNA, lipopolysaccharide (LPS), and insulin, as determined by ELISAs (Figures 4C, 4D, and S3C). A small fraction of all S-binding mAbs showed some cross reactivity with the S protein of two highly prevalent HCoVs (OC43 and HKU1 but not NL63 or 229E). Likely due to the high degree of sequence conservation of the S2 domain, cross reactivity was only observed among S2-reactive mAbs[9] (Figures 4C, 4D, and S3D). These cross-reactive mAbs originated predominantly from high-SHM MBC (Figure 4D) and were identified in two of the four individuals (V01 and V02). The overall scarcity of HCoV cross-reactive MBCs was in line with the lack of a measurable increase in the anti-HCoV serum IgG antibody concentrations after both vaccinations in our donors (Figure S3D).

Because the majority of mAbs in both subsets recognized the RBD, we measured the antigen affinity of the RBD-specific mAbs by surface plasmon resonance (SPR) (Figures 4C and 4D). The measurements confirmed that low-SHM IgG MBC mAbs showed overall better antigen reactivity than mAbs from high-SHM MBCs and that their binding strength and SHM count correlated positively, likely as a result of active affinity maturation in GC reactions (Figures 4E, S3E, and S3F).

Thus, high-binding anti-SARS-CoV-2 S mAbs developed predominantly from low-SHM IgG MBCs by affinity maturation,

whereas high-SHM IgG MBCs mAbs showed overall low antigen binding and antibody affinity, which did not improve over time or after the booster vaccination.

Despite weak S reactivity, pre-existing MBCs quickly differentiate into ASCs upon vaccination

To determine to what degree low- and high-SHM MBCs differentiated into ASCs over the course of the response, we examined the Ig gene repertoire of low- and high-SHM ASCs (Figure S4A). Paired Ig heavy- and light-chain V gene usage and clonal overlap analyses provided evidence for the common origin of ASCs and MBCs with a low SHM count and of ASCs and MBCs with a high SHM load, respectively (Figures 5A and 5B). High-SHM IgG ASCs dominated the response at all time points, although the frequency of low-SHM ASCs increased after each vaccination (Figure 5C). mAbs cloned from low-SHM ASCs showed stronger S binding and the frequency of antigen binders was overall higher in low- compared with high-SHM ASCs, similar to the differences we observed between low- and high-SHM IgG MBCs (Figures 5D and S4B). In line with these findings, low-SHM ASCs showed higher S-barcode read counts and S+ cell frequency compared with their high-SHM counterparts (Figures S4C and S4D).

To be able to link antigen binding to ASC differentiation kinetics, we applied pseudotime analysis based on diffusion distance (Figure 5E). The expression of proliferation markers, B cell markers, and pro-apoptotic genes decreased gradually along the pseudotime trajectory, while PC and survival markers, including *CD138*, increased concomitantly (Figure 5F). Thus, the pseudotime values reflected the ASC maturation from proliferating plasmablasts (PB) to mature PCs over time and was used to define the maturation stages of ASCs with high or low SHM counts (PB, early PC, and mature PC, Figure 5E). Already at I + 1 week, high-SHM IgG ASCs had higher pseudotime values compared with low-SHM IgG ASCs with high and stable frequency of mature PCs over time (Figures 5G and S4E). By contrast, mature PCs were rare among low-SHM IgG ASCs after the first vaccination and increased only slowly, mainly after the boost, concomitant with increases in anti-S serum IgG titers (Figures 5G, S1A, and S4F).

Thus, the data indicate that, in response to the vaccination, S+ high-SHM IgG MBCs expressing weakly binding antibodies developed quickly into non-proliferating mature ASCs. By contrast, low-SHM MBCs with similar antigen binding improved their antibody affinity by SHM in GC reactions before differentiating into proliferating ASCs.

DISCUSSION

Our data demonstrate that the initial anti-S ASC response to mRNA vaccination in SARS-CoV-2-naive individuals is driven by pre-existing MBCs, although the average S-binding strength of their antibodies was not higher than that of newly developing MBCs derived from naive precursors. We have made similar observations in malaria-naive individuals after vaccination with live parasites, suggesting that human MBCs have a high propensity to differentiate into ASCs upon BCR-mediated activation even when they have not previously encountered the stimulating antigen.[28] The high numbers of SHM in the S+ IgG MBCs that responded to SARS-CoV-2 vaccination in our study were comparable with the average SHM counts of the same cell population before the first vaccination, indicating that these cells must have developed prior to the vaccination. Their relatively low SARS-CoV-2 S-protein binding likely reflects weak antigen cross reactivity, a common feature of Ig molecules, including antibodies that have undergone affinity maturation.[29] Given the size of the human MBC pool, cross reactivity in this compartment likely plays an important role in protection from diverse antigenic threats by increasing the number of cells that can be recruited into the response for the rapid production of serum antibodies upon differentiation into ASCs. The low anti-S antibody titers after the prime likely reflect the weak binding properties of these cells compared with the strong binders that develop after the boost from affinity-matured naive precursors.

Numerous studies have illustrated that human MBCs readily respond to antigen-independent polyclonal stimuli and bystander T cell help by proliferation and differentiation into ASCs *in vitro*.[30,31] In particular, IgG class-switched MBCs have been shown to have a lower activation threshold and higher sensitivity to bystander T cell help than IgM MBCs,[32–34] in line with the fact that we did not detect signs for an active participation of IgM MBCs in the anti-S response at serum or cellular level.

The high-SHM MBCs studied here displayed similar S binding compared with the low-SHM MBCs, nevertheless the two subsets differed in their differentiation paths. The strong T cell responses induced by mRNA vaccination might have promoted the fast differentiation of S-reactive IgG MBCs into ASCs, compared with naive B cells, which showed clear signs of affinity maturation in GC reactions.[1,35,36]

Likely due to the highly polyclonal nature of the anti-S response, we did not observe strong signs of clonal expansion among pre-existing high-SHM MBCs over the vaccination course. Instead, the cells upregulated *TXNIP*, IL-9, and IRF4 pathways expression (markers associated with PC differentiation, at least in mice)[23,24] and rapidly differentiated into more terminally differentiated ASCs. The fast development of pre-existing MBCs into ASCs suggests that these cells are the main contributors to the first wave of serum IgG. The fast secretion of low-binding anti-S IgG antibodies by these cells might promote the activation and selection of S-reactive B cells through the formation of immune complexes and subsequent deposition of antigen on follicular dendritic cells in GCs.[37] IgA MBCs may play a similar role because although highly mutated IgA-secreting cells constituted a significant fraction of ASCs, serum anti-S IgA was low—likely because the intramuscular administration of the vaccine failed to induce the *de novo* development of IgA MBCs from naive precursors (Figures S4G and S4H).

The second vaccination induced a strong increase in IgG titers and likely in antibody quality as we did not detect a proportionally strong increase in the frequency of IgG ASCs after the boost. Our data suggest that the high-affinity serum IgG antibodies measured after the second vaccine dose originated predominantly from *de novo* responses of naive B cell precursors, which class-switched and showed clear signs of affinity maturation prior to differentiation into proliferating ASCs.

It remains to be determined whether the fates of the high- and low-SHM MBCs change in response to a second booster. Unfortunately, this could not be addressed here because all

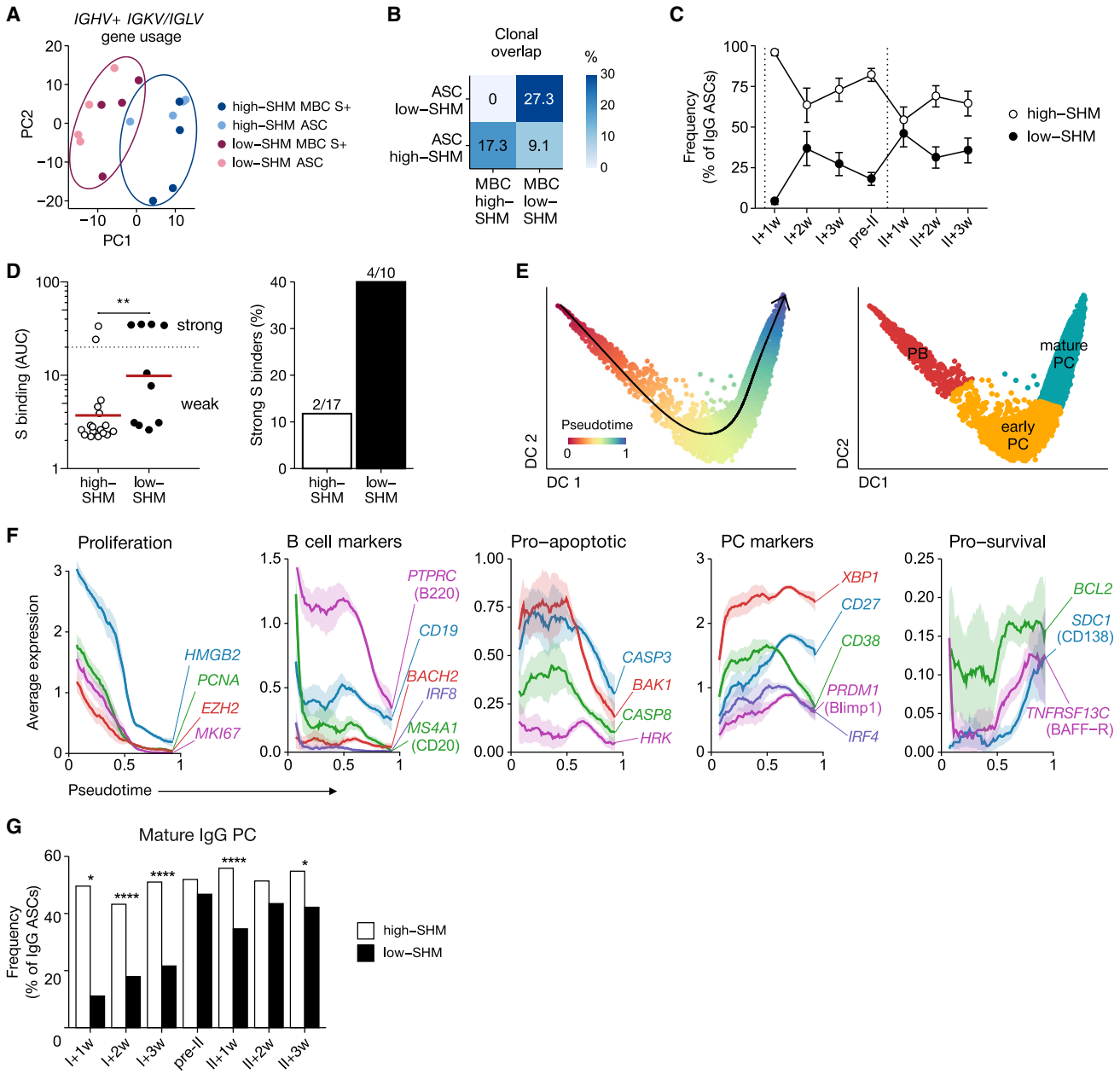

Figure 5. Naive B cells generate less mature but more potent IgG-expressing ASCs compared with pre-existing MBCs

(A) Principal component analysis (PCA) on paired-chain V gene usage of IgM and IgG cells. Dots represent MBCs or ASCs populations from individual donors.

(B) Clonal overlap between IgM or IgG high- and low-SHM S+ MBCs and ASCs.

(C) Frequency of high- and low-SHM IgG ASCs over time. Dotted vertical lines indicate prime and boost.

(D) mAb ELISA AUC values (left) and frequencies of strong binders (right) in ASCs clonally related to low- and high-SHM S+ MBCs. Dotted lines show thresholds for weak- and strong-binding mAbs. Numbers on top of the bars show the numbers of strong binders over the total number of mAbs. Red lines show average.

(E) Diffusion map of ASCs colored by pseudotime (left) or maturation stage (right). PB, plasmablasts (pseudotime $\leqslant$0.33); early PC, early plasma cell (0.33 < pseudotime < 0.66); mature PC, mature plasma cell (pseudotime $\geqslant$0.66).

(F) Expression of genes contributing to mature PC phenotype along the pseudotime trajectory.

(G) Frequency of mature PCs among low- and high-SHM IgG ASCs across time points. *p < 0.05, **p < 0.01, ***p < 0.001, ****p < 0.0001, binomial test (G), two-tailed Mann-Whitney test (D). Error bars display SEM (C).

See also Figure S4.

participants became infected with SARS-CoV-2 before they received a third vaccination. Nevertheless, given the high binding strength of the newly generated MBCs that developed from naive precursors over the course of the two vaccinations, we expect these cells to quickly differentiate into ASCs in any recall response to the same SARS-CoV-2 S antigen. Under these

circumstances, the high-affinity MBCs might suppress *de novo* responses from naive precursors, an effect described as original antigenic sin or, more adequately, as antigenic, immunogenic, or immune imprinting.[38,39]

Our data are in line with previous observations in murine model systems that assessed the fate of MBCs in recall responses.[13–17] Laboratory mice lack pre-existing MBCs under steady-state conditions, likely due to their pathogen-free housing conditions, and therefore cannot fully mimic immune responses in humans. Nevertheless, immunization and infection studies showed that clones without prior GC experience that are likely of naive origin dominated secondary GC reactions, whereas MBCs were overall rare in these anatomical structures and showed no strong signs of re-diversification in recall responses.[13]

Differences in frequency of strongly antigen-reactive germline precursors and in affinity might influence the ratio of naive B cells and MBCs in GCs and their differentiation paths. A better understanding of the mechanisms that control the fate of MBCs and of potential affinity thresholds will be critical to understanding how to drive responses against targets, such as the HIV S protein with low germline precursor frequency, that require high SHM loads for the development of broadly protective antibodies. Promoting long-lasting GC reactions by the continued slow delivery of antigens might help to boost affinity maturation and the quality of humoral immune memory without the need to drive MBC re-entry into GCs.[40,41]

In summary, our study demonstrates that human IgG MBCs have an intrinsic propensity to differentiate into ASCs, and the quality of the response to mRNA vaccination in SARS-CoV-2-naive individuals improves through the clonal selection and affinity maturation of potent S-reactive naive B cell precursors. Our findings demonstrate that the immune imprinting effect that drives MBC fate toward ASC differentiation is not limited to MBCs with high affinity for the recall antigen, as suggested by the original antigenic sin theory.[38,39] Future studies will be necessary to confirm the generalizability of these findings beyond SARS-CoV-2 and to define under which conditions MBCs might remain in or re-enter GCs to improve their antibody quality.

Limitations of the study

A major limitation of our study is the lack of longitudinal data from draining lymph nodes that could provide information about the affinity maturation process of individual clones. It is possible that some pre-existing MBCs in our study participated in GC reactions, although these were likely rare events relative to the GC participation of naive B cell clones, including cells expressing Ig genes associated with S reactivity. Direct sampling of lymph node GC B cells in SARS-CoV-2 vaccinees identified highly mutated clones with strong cross reactivity to S protein from HCoVs, suggesting that these cells represented pre-existing MBCs that had developed in response to prior infections with common cold viruses.[11] Nevertheless, the majority of GC B cells in this study seemed to be SARS-CoV-2 S specific and likely developed from naive precursors because their mutation load was significantly lower than that of clones with HCoV cross reactivity. Access to secondary lymphoid tissue is overall limited in humans. Repeated deep sampling of draining lymph nodes would be necessary to link the GC to the circulating MBC response, ideally at the level of individual clones, to track the cellular evolution process over time.

STAR★METHODS

Detailed methods are provided in the online version of this paper and include the following:

- KEY RESOURCES TABLE
- RESOURCE AVAILABILITY
  - Lead contact
  - Materials availability
  - Data and code availability
- EXPERIMENTAL MODEL AND STUDY PARTICIPANT DETAILS
  - Human materials
  - Cell lines
- METHOD DETAILS
  - Antigens
  - Flow cytometry, cell sorting, and 10x sample preparation
  - Droplet-based single-cell sequencing
  - scRNA-seq processing and analysis
  - Gene expression and signature enrichment analysis
  - BCR repertoire analysis
  - Recombinant monoclonal antibody production
  - Enzyme-linked immunosorbent assay (ELISA)
  - Surface plasmon resonance (SPR)
- QUANTIFICATION AND STATISTICAL ANALYSIS

SUPPLEMENTAL INFORMATION

Supplemental information can be found online at https://doi.org/10.1016/j.immuni.2024.07.023.

ACKNOWLEDGMENTS

The authors thank Theresa Kissel for technical advice related to establishing the high-sensitivity ELISA and Yasmin Bergmann, Christine Niesik, and Dorien Foster (DKFZ) for technical assistance. The authors are grateful to Alessandro Greco and Thomas Höfer (DKFZ) for advice on transcriptome analysis and would like to acknowledge the EMBL Protein Expression and Purification Core Facility, the DKFZ NGS Core Facility, DKFZ single-cell Open Lab (scOpenLab), and the DKFZ/EMBL/Heidelberg University Chemical Biology Core Facility, especially Peter Sehr, for technical assistance and services; Jan-Philipp Mallm for advice on single-cell RNA sequencing (RNA-seq); and Julia Ludwig for helpful discussions. The authors thank the vaccine trial participants for their contribution to the study and Patrick C. Wilson for sharing the SARS-CoV-2 S antigen expression vector originally generated by Florian Krammer. This work was supported by the Helmholtz Association's Initiative and Networking Fund project "Virological and immunological determinants of COVID-19 pathogenesis—lessons to get prepared for future pandemics (KA1-Co-02_CoViPa)." A.O. was supported by the DKFZ International PhD Program.

AUTHOR CONTRIBUTIONS

H.W. conceived the study. Z.L., A.O., R.M., and H.W. designed the experiments. K.B. collected blood samples. J.M. and R.M. isolated PBMCs and plasma. M.v.S. and E.S. provided spike and RBD proteins. Z.L. and F.S. sorted single cells and prepared sequencing libraries. A.O. performed computational analyses. Z.L. expressed monoclonal antibodies. Z.L., O.E.O., and J.M. performed serum and monoclonal antibody assays. Z.L., A.O., and H.W. interpreted the data. Z.L., A.O., and H.W. wrote the paper. H.W. acquired funding and supervised the study. All authors read and approved the final manuscript.

DECLARATION OF INTERESTS

The authors declare no competing interests.

Received: December 18, 2023
Revised: February 2, 2024
Accepted: July 24, 2024
Published: August 20, 2024

REFERENCES

1. Siekevitz, M., Kocks, C., Rajewsky, K., and Dildrop, R. (1987). Analysis of somatic mutation and class switching in naive and memory B cells generating adoptive primary and secondary responses. Cell *48*, 757–770. https://doi.org/10.1016/0092-8674(87)90073-0.
2. Slifka, M.K., Antia, R., Whitmire, J.K., and Ahmed, R. (1998). Humoral immunity due to long-lived plasma cells. Immunity *8*, 363–372. https://doi.org/10.1016/s1074-7613(00)80541-5.
3. Askonas, B.A., and Williamson, A.R. (1972). Dominance of a cell clone forming antibody to DNP. Nature *238*, 339–341. https://doi.org/10.1038/238339a0.
4. Berek, C., Jarvis, J.M., and Milstein, C. (1987). Activation of memory and virgin B cell clones in hyperimmune animals. Eur. J. Immunol. *17*, 1121–1129. https://doi.org/10.1002/eji.1830170808.
5. Weisel, F., and Shlomchik, M. (2017). Memory B Cells of Mice and Humans. Annu. Rev. Immunol. *35*, 255–284. https://doi.org/10.1146/annurev-immunol-041015-055531.
6. Inoue, T., and Kurosaki, T. (2024). Memory B cells. Nat. Rev. Immunol. *24*, 5–17. https://doi.org/10.1038/s41577-023-00897-3.
7. Viant, C., Weymar, G.H.J., Escolano, A., Chen, S., Hartweger, H., Cipolla, M., Gazumyan, A., and Nussenzweig, M.C. (2020). Antibody Affinity Shapes the Choice between Memory and Germinal Center B Cell Fates. Cell *183*, 1298–1311.e11. https://doi.org/10.1016/j.cell.2020.09.063.
8. Brewer, R.C., Ramadoss, N.S., Lahey, L.J., Jahanbani, S., Robinson, W.H., and Lanz, T.V. (2022). BNT162b2 vaccine induces divergent B cell responses to SARS-CoV-2 S1 and S2. Nat. Immunol. *23*, 33–39. https://doi.org/10.1038/s41590-021-01088-9.
9. Ng, K.W., Faulkner, N., Cornish, G.H., Rosa, A., Harvey, R., Hussain, S., Ulferts, R., Earl, C., Wrobel, A.G., Benton, D.J., et al. (2020). Preexisting and de novo humoral immunity to SARS-CoV-2 in humans. Science *370*, 1339–1343. https://doi.org/10.1126/science.abe1107.
10. Kim, W., Zhou, J.Q., Horvath, S.C., Schmitz, A.J., Sturtz, A.J., Lei, T., Liu, Z., Kalaidina, E., Thapa, M., Alsoussi, W.B., et al. (2022). Germinal centre-driven maturation of B cell response to mRNA vaccination. Nature *604*, 141–145. https://doi.org/10.1038/s41586-022-04527-1.
11. Turner, J.S., O'Halloran, J.A., Kalaidina, E., Kim, W., Schmitz, A.J., Zhou, J.Q., Lei, T., Thapa, M., Chen, R.E., Case, J.B., et al. (2021). SARS-CoV-2 mRNA vaccines induce persistent human germinal centre responses. Nature *596*, 109–113. https://doi.org/10.1038/s41586-021-03738-2.
12. McIntire, K.M., Meng, H., Lin, T.H., Kim, W., Moore, N.E., Han, J., McMahon, M., Wang, M., Malladi, S.K., Mohammed, B.M., et al. (2024). Maturation of germinal center B cells after influenza virus vaccination in humans. J. Exp. Med. *221*, e20240668. https://doi.org/10.1084/jem.20240668.
13. Mesin, L., Schiepers, A., Ersching, J., Barbulescu, A., Cavazzoni, C.B., Angelini, A., Okada, T., Kurosaki, T., and Victora, G.D. (2020). Restricted Clonality and Limited Germinal Center Reentry Characterize Memory B Cell Reactivation by Boosting. Cell *180*, 92–106.e11. https://doi.org/10.1016/j.cell.2019.11.032.
14. Zuccarino-Catania, G.V., Sadanand, S., Weisel, F.J., Tomayko, M.M., Meng, H., Kleinstein, S.H., Good-Jacobson, K.L., and Shlomchik, M.J. (2014). CD80 and PD-L2 define functionally distinct memory B cell subsets that are independent of antibody isotype. Nat. Immunol. *15*, 631–637. https://doi.org/10.1038/ni.2914.
15. McHeyzer-Williams, L.J., Milpied, P.J., Okitsu, S.L., and McHeyzer-Williams, M.G. (2015). Class-switched memory B cells remodel BCRs within secondary germinal centers. Nat. Immunol. *16*, 296–305. https://doi.org/10.1038/ni.3095.
16. Pape, K.A., Taylor, J.J., Maul, R.W., Gearhart, P.J., and Jenkins, M.K. (2011). Different B cell populations mediate early and late memory during an endogenous immune response. Science *331*, 1203–1207. https://doi.org/10.1126/science.1201730.
17. Dogan, I., Bertocci, B., Vilmont, V., Delbos, F., Mégret, J., Storck, S., Reynaud, C.A., and Weill, J.C. (2009). Multiple layers of B cell memory with different effector functions. Nat. Immunol. *10*, 1292–1299. https://doi.org/10.1038/ni.1814.
18. Wec, A.Z., Wrapp, D., Herbert, A.S., Maurer, D.P., Haslwanter, D., Sakharkar, M., Jangra, R.K., Dieterle, M.E., Lilov, A., Huang, D., et al. (2020). Broad neutralization of SARS-related viruses by human monoclonal antibodies. Science *369*, 731–736. https://doi.org/10.1126/science.abc7424.
19. Goel, R.R., Apostolidis, S.A., Painter, M.M., Mathew, D., Pattekar, A., Kuthuru, O., Gouma, S., Hicks, P., Meng, W., Rosenfeld, A.M., et al. (2021). Distinct antibody and memory B cell responses in SARS-CoV-2 naïve and recovered individuals following mRNA vaccination. Sci. Immunol. *6*, eabi6950. https://doi.org/10.1126/sciimmunol.abi6950.
20. Ellebedy, A.H., Jackson, K.J.L., Kissick, H.T., Nakaya, H.I., Davis, C.W., Roskin, K.M., McElroy, A.K., Oshansky, C.M., Elbein, R., Thomas, S., and Lyon, G.M. (2016). Defining antigen-specific plasmablast and memory B cell subsets in human blood after viral infection or vaccination. Nat. Immunol. *17*, 1226–1234. https://doi.org/10.1038/ni.3533.
21. Domeier, P.P., Chodisetti, S.B., Soni, C., Schell, S.L., Elias, M.J., Wong, E.B., Cooper, T.K., Kitamura, D., and Rahman, Z.S.M. (2016). IFN-γ receptor and STAT1 signaling in B cells are central to spontaneous germinal center formation and autoimmunity. J. Exp. Med. *213*, 715–732. https://doi.org/10.1084/jem.20151722.
22. Craxton, A., Shu, G., Graves, J.D., Saklatvala, J., Krebs, E.G., and Clark, E.A. (1998). p38 MAPK is required for CD40-induced gene expression and proliferation in B lymphocytes. J. Immunol. *161*, 3225–3236. https://doi.org/10.4049/jimmunol.161.7.3225.
23. Takatsuka, S., Yamada, H., Haniuda, K., Saruwatari, H., Ichihashi, M., Renauld, J.C., and Kitamura, D. (2018). IL-9 receptor signaling in memory B cells regulates humoral recall responses. Nat. Immunol. *19*, 1025–1034. https://doi.org/10.1038/s41590-018-0177-0.
24. Klein, U., Casola, S., Cattoretti, G., Shen, Q., Lia, M., Mo, T., Ludwig, T., Rajewsky, K., and Dalla-Favera, R. (2006). Transcription factor IRF4 controls plasma cell differentiation and class-switch recombination. Nat. Immunol. *7*, 773–782. https://doi.org/10.1038/ni1357.
25. Graham, C., Seow, J., Huettner, I., Khan, H., Kouphou, N., Acors, S., Winstone, H., Pickering, S., Galao, R.P., Dupont, L., and Lista, M.J. (2021). Neutralization potency of monoclonal antibodies recognizing dominant and subdominant epitopes on SARS-CoV-2 Spike is impacted by the B.1.1.7 variant. Immunity *54*, 1276–1289.e6. https://doi.org/10.1016/j.immuni.2021.03.023.
26. Brouwer, P.J.M., Caniels, T.G., van der Straten, K., Snitselaar, J.L., Aldon, Y., Bangaru, S., Torres, J.L., Okba, N.M.A., Claireaux, M., Kerster, G., and Bentlage, A.E. (2020). Potent neutralizing antibodies from COVID-19 patients define multiple targets of vulnerability. Science *369*, 643–650. https://doi.org/10.1126/science.abc5902.
27. Yuan, M., Liu, H., Wu, N.C., Lee, C.D., Zhu, X., Zhao, F., Huang, D., Yu, W., Hua, Y., Tien, H., and Rogers, T.F. (2020). Structural basis of a shared antibody response to SARS-CoV-2. Science *369*, 1119–1123. https://doi.org/10.1126/science.abd2321.
28. Murugan, R., Buchauer, L., Triller, G., Kreschel, C., Costa, G., Pidelaserra Martí, G., Imkeller, K., Busse, C.E., Chakravarty, S., Sim, B.K.L., and Hoffman, S.L. (2018). Clonal selection drives protective memory B cell responses in controlled human malaria infection. Sci. Immunol. *3*, eaap8029. https://doi.org/10.1126/sciimmunol.aap8029.
29. Tiller, T., Tsuiji, M., Yurasov, S., Velinzon, K., Nussenzweig, M.C., and Wardemann, H. (2007). Autoreactivity in human IgG+ memory B cells. Immunity *26*, 205–213. https://doi.org/10.1016/j.immuni.2007.01.009.
30. Tangye, S.G., Avery, D.T., Deenick, E.K., and Hodgkin, P.D. (2003). Intrinsic differences in the proliferation of naive and memory human B cells

as a mechanism for enhanced secondary immune responses. J. Immunol. *170*, 686–694. https://doi.org/10.4049/jimmunol.170.2.686.

31. Good, K.L., Avery, D.T., and Tangye, S.G. (2009). Resting human memory B cells are intrinsically programmed for enhanced survival and responsiveness to diverse stimuli compared to naive B cells. J. Immunol. *182*, 890–901. https://doi.org/10.4049/jimmunol.182.2.890.
32. Wan, Z., Chen, X., Chen, H., Ji, Q., Chen, Y., Wang, J., Cao, Y., Wang, F., Lou, J., Tang, Z., and Liu, W. (2015). The activation of IgM- or isotype-switched IgG- and IgE-BCR exhibits distinct mechanical force sensitivity and threshold. eLife *4*, e06925. https://doi.org/10.7554/eLife.06925.
33. Liu, W., Meckel, T., Tolar, P., Sohn, H.W., and Pierce, S.K. (2010). Intrinsic properties of immunoglobulin IgG1 isotype-switched B cell receptors promote microclustering and the initiation of signaling. Immunity *32*, 778–789. https://doi.org/10.1016/j.immuni.2010.06.006.
34. Bernasconi, N.L., Traggiai, E., and Lanzavecchia, A. (2002). Maintenance of serological memory by polyclonal activation of human memory B cells. Science *298*, 2199–2202. https://doi.org/10.1126/science.1076071.
35. Mudd, P.A., Minervina, A.A., Pogorelyy, M.V., Turner, J.S., Kim, W., Kalaidina, E., Petersen, J., Schmitz, A.J., Lei, T., Haile, A., and Kirk, A.M. (2022). SARS-CoV-2 mRNA vaccination elicits a robust and persistent T follicular helper cell response in humans. Cell *185*, 603–613.e15. https://doi.org/10.1016/j.cell.2021.12.026.
36. Sahin, U., Muik, A., Derhovanessian, E., Vogler, I., Kranz, L.M., Vormehr, M., Baum, A., Pascal, K., Quandt, J., Maurus, D., and Brachtendorf, S. (2020). COVID-19 vaccine BNT162b1 elicits human antibody and TH1 T cell responses. Nature *586*, 594–599. https://doi.org/10.1038/s41586-020-2814-7.
37. Zhang, Y., Garcia-Ibanez, L., and Toellner, K.M. (2016). Regulation of germinal center B-cell differentiation. Immunol. Rev. *270*, 8–19. https://doi.org/10.1111/imr.12396.
38. Francis, T. (1960). On the Doctrine of Original Antigenic Sin. Proc. Am. Philos. Soc. *104*, 572–578.
39. Koutsakos, M., and Ellebedy, A.H. (2023). Immunological imprinting: Understanding COVID-19. Immunity *56*, 909–913. https://doi.org/10.1016/j.immuni.2023.04.012.
40. Cirelli, K.M., Carnathan, D.G., Nogal, B., Martin, J.T., Rodriguez, O.L., Upadhyay, A.A., Enemuo, C.A., Gebru, E.H., Choe, Y., Viviano, F., and Nakao, C. (2019). Slow Delivery Immunization Enhances HIV Neutralizing Antibody and Germinal Center Responses via Modulation of Immunodominance. Cell *177*, 1153–1171.e28. https://doi.org/10.1016/j.cell.2019.04.012.
41. Gale, E.C., Powell, A.E., Roth, G.A., Meany, E.L., Yan, J., Ou, B.S., Grosskopf, A.K., Adamska, J., Picece, V.C.T.M., d'Aquino, A.I., and Pulendran, B. (2021). Hydrogel-Based Slow Release of a Receptor-Binding Domain Subunit Vaccine Elicits Neutralizing Antibody Responses Against SARS-CoV-2. Adv. Mater. *33*, e2104362. https://doi.org/10.1002/adma.202104362.
42. Tiller, T., Meffre, E., Yurasov, S., Tsuiji, M., Nussenzweig, M.C., and Wardemann, H. (2008). Efficient generation of monoclonal antibodies from single human B cells by single cell RT-PCR and expression vector cloning. J. Immunol. Methods *329*, 112–124. https://doi.org/10.1016/j.jim.2007.09.017.
43. Amanat, F., Stadlbauer, D., Strohmeier, S., Nguyen, T.H.O., Chromikova, V., McMahon, M., Jiang, K., Arunkumar, G.A., Jurczyszak, D., Polanco, J., and Bermudez-Gonzalez, M. (2020). A serological assay to detect SARS-CoV-2 seroconversion in humans. Nat. Med. *26*, 1033–1036. https://doi.org/10.1038/s41591-020-0913-5.
44. Sokal, A., Chappert, P., Barba-Spaeth, G., Roeser, A., Fourati, S., Azzaoui, I., Vandenberghe, A., Fernandez, I., Meola, A., Bouvier-Alias, M., and Crickx, E. (2021). Maturation and persistence of the anti-SARS-CoV-2 memory B cell response. Cell *184*, 1201–1213.e14. https://doi.org/10.1016/j.cell.2021.01.050.
45. Murugan, R., Scally, S.W., Costa, G., Mustafa, G., Thai, E., Decker, T., Bosch, A., Prieto, K., Levashina, E.A., Julien, J.P., and Wardemann, H. (2020). Evolution of protective human antibodies against Plasmodium falciparum circumsporozoite protein repeat motifs. Nat. Med. *26*, 1135–1145. https://doi.org/10.1038/s41591-020-0881-9.
46. Pinto, D., Park, Y.J., Beltramello, M., Walls, A.C., Tortorici, M.A., Bianchi, S., Jaconi, S., Culap, K., Zatta, F., De Marco, A., and Peter, A. (2020). Cross-neutralization of SARS-CoV-2 by a human monoclonal SARS-CoV antibody. Nature *583*, 290–295. https://doi.org/10.1038/s41586-020-2349-y.
47. Wardemann, H., Yurasov, S., Schaefer, A., Young, J.W., Meffre, E., and Nussenzweig, M.C. (2003). Predominant autoantibody production by early human B cell precursors. Science *301*, 1374–1377. https://doi.org/10.1126/science.1086907.
48. Meffre, E., Schaefer, A., Wardemann, H., Wilson, P., Davis, E., and Nussenzweig, M.C. (2004). Surrogate light chain expressing human peripheral B cells produce self-reactive antibodies. J. Exp. Med. *199*, 145–150.
49. Oludada, O.E., Costa, G., Burn Aschner, C., Obraztsova, A.S., Prieto, K., Canetta, C., Hoffman, S.L., Kremsner, P.G., Mordmüller, B., Murugan, R., and Julien, J.P. (2023). Molecular and functional properties of human Plasmodium falciparum CSP C-terminus antibodies. EMBO Mol. Med. *15*, e17454. https://doi.org/10.15252/emmm.202317454.

STAR★METHODS

KEY RESOURCES TABLE

REAGENT or RESOURCE	SOURCE	IDENTIFIER
Antibodies		
Brilliant Violet 785™ anti-human CD19 Antibody (Clone HIB19)	BioLegend	Cat# 302240; RRID: AB_2563442
PE/Cyanine7 anti-human CD27 Antibody (Clone 0323)	BioLegend	Cat# 302838; RRID: AB_2561919
BD Horizon™ BV605 Mouse Anti-Human CD38 (Clone HB7)	BD Biosciences	Cat# 562666; RRID: AB_2313578
BD OptiBuild™ BV510 Mouse Anti-Human CD71 (Clone L01.1)	BD Biosciences	Cat# 744926; RRID: AB_2742586
CD3 Monoclonal Antibody, APC-eFluor™ 780 (Clone OKT3)	eBioscience	Cat# 47-0037-41, RRID: AB_2573936
CD8a Monoclonal Antibody, APC-eFluor™ 780 (Clone OKT8)	eBioscience	Cat# 47-0086-42, RRID: AB_2573945
CD14 Monoclonal Antibody, APC-eFluor™ 780 (Clone 61D3)	eBioscience	Cat# 47-0149-42; RRID: AB_1834358
CD16 Monoclonal Antibody, APC-eFluor™ 780 (Clone CB16)	eBioscience	Cat# 47-0168-41; RRID: AB_11219083
TotalSeq™-C0251 anti-human Hashtag 1 Antibody (Clone LNH-94)	BioLegend	Cat# 394661; RRID: AB_2801031
TotalSeq™-C0252 anti-human Hashtag 2 Antibody (Clone LNH-94)	BioLegend	Cat# 394663; RRID: AB_2801032
TotalSeq™-C0253 anti-human Hashtag 3 Antibody (Clone LNH-94)	BioLegend	Cat# 394665; RRID: AB_2801033
TotalSeq™-C0254 anti-human Hashtag 4 Antibody (Clone LNH-94)	BioLegend	Cat# 394667; RRID: AB_2801034
TotalSeq™-C0255 anti-human Hashtag 5 Antibody (Clone LNH-94)	BioLegend	Cat# 394669; RRID: AB_2801035
TotalSeq™-C0256 anti-human Hashtag 6 Antibody (Clone LNH-94)	BioLegend	Cat# 394671; RRID: AB_2820042
TotalSeq™-C0257 anti-human Hashtag 7 Antibody (Clone LNH-94)	BioLegend	Cat# 394673; RRID: AB_2820043
TotalSeq™-C0258 anti-human Hashtag 8 Antibody (Clone LNH-94)	BioLegend	Cat# 394675; RRID: AB_2820044
TotalSeq™-C0259 anti-human Hashtag 9 Antibody (Clone LNH-94)	BioLegend	Cat# 394677; RRID: AB_2820045
TotalSeq™-C0260 anti-human Hashtag 10 Antibody (Clone LNH-94)	BioLegend	Cat# 394679; RRID: AB_2820046
TotalSeq™-C0262 anti-human Hashtag 12 Antibody (Clone LNH-94)	BioLegend	Cat# 394683; RRID: AB_2904413
TotalSeq™-C0263 anti-human Hashtag 13 Antibody (Clone LNH-94)	BioLegend	Cat# 394685; RRID: AB_2904414
TotalSeq™-C0951 PE Streptavidin	BioLegend	Cat# 405261
TotalSeq™-C0956 APC Streptavidin	BioLegend	Cat# 405283
FITC Streptavidin	BioLegend	Cat# 405201
Biological samples		
Human Peripheral blood mononuclear cells (PBMCs)	This paper	S-0001-2022
Chemicals, peptides, and recombinant proteins		
7-AAD	Invitrogen	Cat# A1310
FreeStyle™ 293 Expression Medium	Thermo Fisher	Cat# 12338018
RPMI 1640 Medium	Thermo Fisher	Cat# 31870025
Human TruStain FcX™ (Fc Receptor Blocking Solution)	BioLegend	Cat# 422302; RRID: AB_2818986
Phosphate Buffered Saline (PBS)	Thermo Fisher	Cat# BP39920
Fetal Bovine Serum (FBS)	Thermo Fisher	Cat# 10270106
Bovine serum albumin (BSA)	ROTH	Cat# 8076.5
HCoV-HKU1 Spike protein	Sino Biological	Cat# 40606-V08B
HCoV-OC43 Spike protein	Sino Biological	Cat# 40607-V08B
HCoV-NL63 Spike protein	Sino Biological	Cat# 40604-V08B
HCoV-229E Spike protein	Sino Biological	Cat# 40605-V08B
SARS-CoV-2 Spike S1-His Recombinant Protein	Sino Biological	Cat# 40591-V08B1
SARS-CoV-2 Spike S2 ECD-Fc Recombinant Protein	Sino Biological	Cat# 40590-V02H
Insulin	Sigma-Aldrich	Cat# I9278-5ML
Lipopolysaccharides (LPS)	Sigma-Aldrich	Cat# L2637-5MG
dsDNA	Sigma-Aldrich	Cat# D8515-1G
EDTA	PanReac AppliChem	Cat# A4892
Sensor Chip CM5	GE Healthcare	Cat# BR100530

(*Continued on next page*)

Continued

REAGENT or RESOURCE	SOURCE	IDENTIFIER
ABTS tablets	Roche	Cat# 11112422001
Tween-20	ROTH	Cat# 9127.2
Critical commercial assays		
EZ-Link™ NHS-Biotin	Thermo Fisher	Cat# 20217
Pierce™ Biotin Quantitation Kit	Thermo Fisher	Cat# 28005
Pierce™ BCA Protein Assay Kits	Thermo Fisher	Cat# 23225
NEBuilder® HiFi DNA Assembly Cloning Kit	New England Biolabs	Cat# E2621L
Chromium Next GEM Single Cell 5' Kit v2, 4 rxns	10x Genomics	Cat# 1000265
Chromium Next GEM Chip K Single Cell Kit, 48 rxns	10x Genomics	Cat# 1000286
Chromium Single Cell Human BCR Amplification Kit, 16 rxns	10x Genomics	Cat# 1000253
5' Feature Barcode Kit, 16 rxns	10x Genomics	Cat# 1000256
Library Construction Kit, 16 rxns	10x Genomics	Cat# 1000190
Dual Index Kit TT Set A, 96 rxns	10x Genomics	Cat# 1000215
Dual Index Kit TN Set A, 96 rxns	Biocrates	Cat# 1000250
NovaSeq 6000 S4 Reagent Kit v1.5 (300 cycles)	Illumina	Cat# 20028312
Deposited data		
Single cell RNA-seq data	This paper	GEO: GSE244297
Experimental models: Cell lines		
FreeStyle™ 293-F cells	Thermo Fisher	Cat# R790-07
Recombinant DNA		
IGγ1-, IGκ- or IGλ-expression vectors	Tiller et al.[42]	N/A
Plasmid encoding SARS-CoV-2 Wu01 S ectodomain (amino acids 1-1213 of SARS-CoV-2 S)	Amanat et al.[43]	N/A
Plasmid encoding SARS-CoV-2 Wu01 RBD (amino acids 319-541 of SARS-CoV-2 S)	Amanat et al.[43]	N/A
Software and algorithms		
FlowJo v10.7.2	Tree Star	https://www.flowjo.com/solutions/flowjo/downloads
Prism v9.5.1	GraphPad Software	http://www.graphpad.com/
Biacore™ T200 Software v2.0	Cytiva	https://www.cytivalifesciences.com/en/us
BD FACSDiva v8.0.1	Becton Dickinson	Cat# 659528
bcl-convert v3.9.3	Illumina	https://emea.support.illumina.com/sequencing/sequencing_software/bcl-convert.html
Cell Ranger v6.1.2	10x Genomics	https://www.10xgenomics.com/support/software/cell-ranger/latest
R v4.3.1	R Foundation	https://www.r-project.org/
Ingenuity Pathway Analysis	QIAGEN	https://digitalinsights.qiagen.com/products-overview/discovery-insights-portfolio/analysis-and-visualization/qiagen-ipa/?cmpid=QDI_GA_DISC_IPA&gad_source=1&gclid=Cj0KCQjw_qexBhCoARIsAFgBleu7fsyt0inUtq4TfHJmtTkzpAi3R6isAKk6H4UYgUGbUpFdJRte0HcaAp2lEALw_wcB
IgBLAST v1.20.0	NCBI	https://ftp.ncbi.nih.gov/blast/executables/igblast/release/LATEST/

(*Continued on next page*)

Continued

REAGENT or RESOURCE	SOURCE	IDENTIFIER
RAxML v8	Scientific Computing Group, Heidelberg Institute for Theoretical Studies	https://cme.h-its.org/exelixis/web/software/raxml/
R scripts to reproduce the analysis	This paper	Zenodo: https://doi.org/10.5281/zenodo.11519186

RESOURCE AVAILABILITY

Lead contact

Further information and requests for reagents and resources should be directed to and will be fulfilled by the lead contact, Hedda Wardemann (h.wardemann@dkfz.de).

Materials availability

This study did not generate new unique reagents.

Data and code availability

- The raw and processed sequence data have been deposited in GEO and are publicly available from the date of publication. Accession numbers are listed in the key resources table.
- The code for transcriptome and BCR analysis has been deposited in Github and is publicly available as of the date of publication. DOIs are listed in the key resources table.
- Any additional information required to reanalyze the data reported in this paper is available from the lead contact upon request.

EXPERIMENTAL MODEL AND STUDY PARTICIPANT DETAILS

Human materials

This study was approved by the ethics committee of the medical faculty of the University of Heidelberg (S-0001-2022). It is listed under DRKS00028174 in the German Clinical Trials Register and International Clinical Trials Registry Platform. Written consent was obtained from all participants. The study was conducted according to the principles of the Declaration of Helsinki and also conformed to the principles set out in the Department of Health and Human Services Belmont Report. Five healthy donors were enrolled who received two doses of BNT162b2 mRNA SARS-CoV-2 vaccine (Comirnaty®) that encodes a prefusion stabilized, membrane-anchored SARS-CoV-2 full-length Spike protein (Table S1). Peripheral blood samples were collected one day before, one, two and three weeks after each of the two vaccinations. Peripheral blood mononuclear cells (PBMCs) were isolated using Ficoll gradient density centrifugation, frozen in 10% dimethyl sulfoxide in fetal calf serum and stored in liquid nitrogen until further use.

Cell lines

HEK293-F cells (Thermo Fisher) were used in the production of monoclonal antibodies. Cells were maintained at 37°C and 8% CO2 in FreeStyle 293 Expression Medium (Thermo Fisher) under constant shaking at 180 rpm. Supernatants were harvested by centrifugation seven days after transfection.

METHOD DETAILS

Antigens

The mammalian expression vector encoding SARS-CoV-2 Spike protein or RBD derived from the first virus isolate, Wuhan-Hu-1 was previously described.[43] Two modifications were introduced to Spike protein sequences to stabilize the trimer in the pre-fusion conformation. Spike and RBD were expressed in HEK293-F cells and purified by NI-IMAC resin. For constructing baits for flow cytometry, purified SARS-CoV-2 Spike and RBD were biotinylated using the EZ-Link NHS-Biotin (Thermo Fisher Scientific) following the manufacturer's instructions. The mole-to-mole ratio of biotin to protein was quantified using the Pierce Biotin Quantitation Kit (Thermo Fisher Scientific). Biotinylated Spike was conjugated to streptavidin-FITC (BioLegend) and streptavidin-PE (BioLegend, TotalSeq™-C0951) and RBD to streptavidin-APC (BioLegend, TotalSeq™-C0956) overnight at 4°C.

Flow cytometry, cell sorting, and 10x sample preparation

PBMCs were thawed at 37°C and washed twice with RPMI (Gibco). Cells were incubated for 10 min at 4 °C with Fc receptor block (TruStain FcX, BioLegend, 1:10). Cells were washed and incubated in FACS buffer (1xPBS, 2%FCS) with the following anti-human antibodies: CD19-BV785 (BioLegend, 1:10), CD3-APC-eFluor 780 (Invitrogen, 1:200), CD8-APC-eFluor 780 (Invitrogen, 1:200),

CD14-APC-eFluor 780 (Invitrogen, 1:200), CD16-APC-eFluor 780 (Invitrogen, 1:200), CD27-PE-Cy7 (BioLegend, 1:20), CD38-BV605 (BD Biosciences, 1:20), CD71-BV510 (BD Biosciences, 1:10), TotalSeq-C hashtag antibodies 1–12 (BioLegend, 1:100) and Spike and RBD antigen tetramers. Afterwards, cells were washed and stained with 7-Aminoactinomycin D (7AAD) (Invitrogen, 1:400) that was used as a dead cell marker. Single cells were sorted with FACSAria III (BD Biosciences) into cooled 1.5-ml tubes. FACS data were collected with the BD FACSDiva (v8.0.1) software and analyzed using FlowJo v10.7.2 (Tree Star).

Droplet-based single-cell sequencing

Sorted single cells were captured using Chromium controller (10x Genomics) according to the Chromium Single Cell 5' Reagent Kit (CG000330 Rev C) protocols. Briefly, the cell suspension was loaded onto the controller to encapsulate single cells into droplets with barcoded gel beads using Gel Bead kit v2 (10x Genomics, 1000265) and Next GEM Chip K Single-Cell kit (10x Genomics, 1000286). Up to 20,000 cells were added to each channel with an expected recovery of 8,000 cells. Captured cells were lysed and the released RNA was barcoded through reverse transcription. The 5′ gene expression (GEX) libraries, V(D)J libraries (10x Genomics, 1000190) and cell surface protein libraries (10x Genomics, 1000256) were prepared according to the manufacturer's protocols. Library quality was assessed using a 2200 TapeStation (Agilent). Libraries were sequenced on an Illumina NovaSeq6000 platform (150+150 bp paired read length).

scRNA-seq processing and analysis

Libraries were demultiplexed using bcl-convert v3.9.3. Reads were mapped to the human genome (GRCh38-2020-A) using 10x Genomics Cell Ranger v6.1.2 multi. Hashtag-based sample demultiplexing was done using hashedDrops function from DropletUtils R package v1.19.3. The following cells were filtered out: no confident sample assignment or classified as doublet based on the hashtag read count, >1% of hemoglobin gene expression, outliers in the distribution of mitochondrial gene expression or the number of detected genes. Outliers were detected based on the median absolute deviation using isOutlier function from scuttle package v1.9.4. Before normalization, read counts from the following sets of genes were combined into single features: Ig V, D and J genes; Ig constant genes of all isotypes; small and large ribosomal subunit protein genes; HLAI genes; HLAII genes excluding HLA-DO and HLA-DM. The exclusion of these genes from the dataset did not result in a significant alteration in cell clustering, thus they were retained in the dataset. Data normalization and variable gene selection was done using SCTransform from Seurat package v4.3.0. Principal component analysis, UMAP embedding, nearest neighbor graph construction and clustering were done using standard Seurat functions. Clusters of cells expressing non-B cell markers (*LYZ, CD14, CD68, GNLY, GZMA, CD3E, CD3G, CD4*) were removed and the data was re-normalized and re-clustered. Diffusion map embeddings were calculated using destiny R package v3.8.1. Single-cell pseudotime trajectory was calculated with slingshot R package v2.7.0 based on the clusters defined with Seurat. S-reactive cells were defined based on having read count above the threshold for either Spike or RBD antigen barcode. Thresholds were defined based on the optimal separation of positive and negative cell populations.

Gene expression and signature enrichment analysis

Differentially expressed genes were detected using FindMarkers with Benjamini-Hochberg multiple testing correction. The genes were considered differentially expressed if p.adjusted <0.05 and average fold change >1.3. Ingenuity Pathway Analysis (IPA) was performed using avg_logFC values of all differentially expressed genes. BCR signaling pathway expression was quantified using AUCell v1.21.1.

BCR repertoire analysis

Full-length V(D)J contigs were assembled with Cell Ranger and aligned to the IMGT reference using IgBLAST v1.20.0 and all downstream analyses were done with R. Contigs were filtered using the following criteria: cells passed the transcriptome quality control, V(D)J information is available for one heavy and one light chain, classified as full-length, productive and high-confidence by Cell Ranger. Clones were defined as groups of cells sharing at least one V and J genes in the top-3 alignment hits and having CDR3 nucleotide sequence similarity >80%. The similarity threshold was defined based on the distribution of nearest-neighbor similarity. After defining clones, all cells in a clone were assigned the V and J genes used by the majority of cells in a clone. To reconstruct phylogenetic trees, merged heavy and light chain V gene sequences were aligned using ClustalW method implemented in msa R package v1.31.7. Phylogenetic trees were reconstructed by RAxML v8 using germline sequence as an outgroup for each clone. Trees were visualized using ggtree v3.7.2. Low- and high-SHM cells were separated based on the bimodal distribution of SHM counts.[44] SHM count threshold was set at a saddle point separating the first density peak from the rest of the distribution individually for each time point (Figure S2A).

Recombinant monoclonal antibody production

A representative set of antibodies was selected to reflect V gene usage, SHM counts, clone size and the variability in S-barcode read counts within the selected B cell populations. The selected pairs of Ig heavy and light chain gene sequences were synthesized by Twist Bioscience and cloned into IgG1 and Igλ or Igκ expression vectors (Addgene number 80795, 80796 and 99575, respectively). Plasmids encoding paired Ig heavy and light chains were co-transfected into human embryonic kidney (HEK) 293F cells (Thermo Fisher Scientific) for recombinant mAb production. HEK293F cells were cultured in FreeStyle 293-F medium (Gibco) according to the manufacturer's protocol.

Enzyme-linked immunosorbent assay (ELISA)

ELISAs were performed as previously described.[45] In brief, 384-well high-binding polystyrene plates (Corning) were coated overnight at 4°C with Spike (4μg/ml), HCoV-HKU1 (4μg/ml), HCoV-OC43 (4μg/ml; Sino Biological), HCoV-229E (4μg/ml; Sino Biological), HCoV-NL63 (4μg/ml; Sino Biological), S1 (4μg/ml; Sino Biological), S2 (4μg/ml; Sino Biological), RBD (4μg/ml), double-stranded DNA (dsDNA) (10μg/ml; Sigma), human insulin (5μg/ml; Sigma), or lipopolysaccharide (LPS) (10μg/ml; Sigma) in PBS. Plates were washed three times with washing buffer (1× PBS with 0.05% Tween-20 (Sigma-Aldrich)) or with Millipore water (high sensitivity ELISA and polyreactivity ELISA). ELISA plates were blocked for one hour at room temperature with 2% or 4% bovine serum albumin (BSA) in PBS (regular ELISA or serum ELISA and high sensitivity ELISA, respectively), or blocking buffer (0.05% Tween-20 and 0.01 M EDTA in PBS; polyreactivity ELISA). Immediately after blocking, serially diluted serum samples at an initial dilution of 1:200 in 1% BSA with PBS, or mAbs at a starting concentration of 10 μg/ml, or 1 μg/ml (polyreactivity ELISA) were loaded on the plate and incubated for two hours at room temperature. Plates were washed three times with washing buffer and then incubated with anti-human IgG, IgA, or IgM secondary antibody conjugated to horseradish peroxidase at 1:1000 (Jackson ImmunoResearch) in the corresponding blocking buffer (1× PBS with 0.05% Tween-20 and 0.01 M EDTA). For high-sensitivity ELISAs, mAbs were pre-incubated with the polyclonal secondary antibody for one hour at room temperature prior to loading on the antigen coated plates to form high-avidity complexes. Plates were developed by addition of the 1-Step™ ABTS substrate (Roche). mAbs S309[46] and mGO53[47] were used as positive and negative controls, respectively. For polyreactivity ELISAs, mAbs ED38[48] and mGO53 were used as positive and negative controls, respectively. Area under the curve (AUC) values were calculated using GraphPad Prism v9 (GraphPad) or R v4.3.1.

Surface plasmon resonance (SPR)

SPR measurements were performed using a Biacore T200 (GE Health-care) instrument docked with Series S Sensor Chip CM5 (GE Healthcare), as previously described.[49] Briefly, anti-human Igκ and Igλ antibodies were immobilized on the chip using an amine coupling-based human antibody Fab capture kit. Hepes (10 mM) with 150 mM NaCl at pH 7.4 was used as a running buffer. Equal concentrations of the sample antibody and isotype control (mGO53)[47] were captured in the sample and reference flow cells, respectively. Running buffer was injected at a rate of 10 μl/min for 20 min to stabilize the flow cells. RBD at 0.02, 0.08, 0.31, 1.25 and 5 μM in running buffer was injected at a rate of 30 μl/min. The flow cells were regenerated with 3 M $MgCl_2$. Steady-state dissociation constants were calculated using BIACORE T200 software V2.0.

QUANTIFICATION AND STATISTICAL ANALYSIS

Statistical analyses were performed using R v4.3.1 or Prism v9 (GraphPad) using tests described in the figure legends. All experiments were performed at least in duplicate.